Journal of ELECTRONIC MATERIALS, Vol. 47, No. 7, 2018
https://doi.org/10.1007/s11664-018-6199-4

Effect of Post-annealing on the Electrochromic Properties of Layer-by-Layer Arrangement FTO-WO_3-Ag-WO_3-Ag

S. HOSEINZADEH,[1] R. GHASEMIASL,[1] A. BAHARI,[2,4] and A.H. RAMEZANI[3]

1.—Department of Mechanical Engineering, West Tehran Branch, Islamic Azad University, Tehran, Iran. 2.—Faculty of Basic Sciences, Department of Physics, University of Mazandaran, Babolsar, Iran. 3.—Department of Physics, West Tehran Branch, Islamic Azad University, Tehran, Iran. 4.—e-mail: a.bahari@umz.ac.ir

In the current study, composites of tungsten trioxide ($W0_3$) and silver (Ag) are deposited in a layer-by-layer electrochromic (EC) arrangement onto a fluorine-doped tin oxide coated glass substrate. Tungsten oxide nanoparticles are an *n*-type semiconductor that can be used as EC cathode material. Nano-sized silver is a metal that can serve as an electron trap center that facilitates charge departure. In this method, the WO_3 and Ag nanoparticle powder were deposited by physical vapor deposition onto the glass substrate. The fabricated electrochromic devices (ECD) were post-annealed to examine the effect of temperature on their EC properties. The morphology of the thin film was characterized by scanning electron microscopy and atomic force microscopy. Structural analysis showed that the addition of silver dopant increased the size of the aggregation of the film. The film had an average approximate roughness of about 17.8 nm. The electro-optical properties of the thin film were investigated using cyclic voltammetry and UV–visible spectroscopy to compare the effects of different post-annealing temperatures. The ECD showed that annealing at 200°C provided better conductivity (maximum current of about 90 mA in the oxidation state) and change of transmittance (ΔT = 90% at the continuous switching step) than did the other thin films. The optical band gaps of the thin film showed that it allowed direct transition at 3.85 eV. The EC properties of these combinations of coloration efficiency and response time indicate that the WO_3-Ag-WO_3-Ag arrangement is a promising candidate for use in such ECDs.

Key words: Nanocomposite, electrochromic device, tungsten oxide, silver, thin film

INTRODUCTION

A substantial amount of research has investigated nanochip electrodes and electrochromic cathode materials.[1–6] Nanoelectronic devices, such as complementary metal oxide semiconductor transistors, organic field effect transistors and organic light emitting diode devices, require an electrode with a high-grade contact point in a particular carrier flux tube or channel. Other devices, such as a cathode deposited onto a fluorine-doped tin oxide (FTO) coating of a glass substrate by physical vapor deposition (PVD), require more trap centers as well as cathodes for electrochromic (EC) and nanodevices.[7–13]

As an inorganic material, tungsten oxide (WO_3) is the most widely studied EC material, and it also has had the most significant commercial uptake.[14] Furthermore, WO_3 is a nontoxic material with a good response time that features intercalation properties (H^+, Li^+, Na^+, and K^+), coloration efficiency and desirable optical properties.[3,15] Tungsten oxide is an

(Received April 18, 2017; accepted March 2, 2018; published online March 13, 2018)

n-type semiconductor with a cubic structure that has attractive characteristics such as a high melting point, high mechanical and chemical stability, high thermal conductivity and low electrical resistivity. This makes it possible to use it as a diffusion barrier for electrochromic devices (ECD).[13–16] WO_3 deposition can be tuned to achieve a wide range of electrical properties by varying the thin film stoichiometry to achieve high transparency, and it is an excellent electron carrier.[4,17] WO_3 can be used for a number of optoelectronic functions. Nano-sized elements such as copper, silver, gold, tantalum, nickel and titanium have been tested as dopants with WO_3. This procedure elevates the electro-optical and EC properties and reduces recombination of the charge carriers.[18–29]

In the present work, the effects of Ag doping on the structural, optical and electrical properties of WO_3 thin film were investigated. The tungsten and silver powders were deposited on FTO-coated glass to form a layer-by-layer structure through physical vapor deposition (PVD). The FTO-WO_3-Ag-WO_3-A thin film was prepared and the post-annealing processes were done at 100°C, 200°C and 500°C to study the effect of post-annealing temperature on the EC properties of the structure. The molecular and morphological structures of the sample were determined by x-ray diffraction (XRD), scanning electron microscopy (SEM) and atomic force microscopy (AFM). The electro-optical properties of the sample were verified by cyclic voltammetry (CV), UV–visible photo spectrometry and current curves to demonstrate the EC properties of coloration efficiency (CE), reversible color (RC) change and response time (RT).

EXPERIMENTAL

Materials

Tungsten oxide (WO_3) powder, Ag nanoparticle powder, lithium perchlorate, propylene carbonate (PC), hydrochloric acid, ethanol and acetone were purchased from Merck. The microscope glass slides (FTO-coated glass) were acquired and cut into small pieces with the size of 2×0.9 cm^2.

Preparation of WO_3-Ag-WO_3-Ag Nanocomposite Layers

A PVD apparatus (Meca; France) equipped with thickness gauging worked at 1.333 kPa was used to deposit the thin film. The FTO-coated glass slides were first washed with detergent and deionized water. They were then cleaned in an ultrasonic bath with ethanol, 0.1 M HCl and acetone for 15 min at room temperature. Parts of the FTO surface were masked as a conducting electrode to prevent deposition. To began the deposition operation, sufficient amounts of WO_3 and Ag powder were used to fill separate tungsten boats in the PVD apparatus.

A digital monitor (Alcatel) was used to monitor the increase in the rate of deposition, thickness and current over time. The WO_3 nanoparticle powder was deposited at a rate of 0.3 (Å s^{-1}) in a vacuum onto the FTO substrate to achieve a film thickness of 200 nm after 90 min (Table I). The Ag nanoparticle powder had previously been deposited to reach 1 nm for 1 min. After switching the target to the boat containing WO_3, a thickness of 3 nm was deposited onto the existing layers for 5 min. The layer of Ag nanoparticles was deposited at a rate of 0.1 (Å s^{-1}) for 1 min (Table I).

Table I. Current and deposition rate changes of the WO_3 and Ag nanoparticles versus its thickness growth during deposition process time

Sample	Time (min)	Current (A)	Rate (Å s^{-1})	Thickness (Å)
WO_3	0	132	0.1	5
WO_3	15	155	0.2	121
WO_3	30	155	0.3	313
WO_3	45	160	0.3	678
WO_3	60	167	0.3	1043
WO_3	75	170	0.4	1481
WO_3	90	170	0.4	2000
Ag	0	113	0.1	3
Ag	1	113	0.1	6
Ag	2	113	0.1	10
WO_3	0	160	0.1	3
WO_3	3	113	0.1	15
WO_3	5	113	0.1	30
Ag	0	113	0.1	2
Ag	1	153	0.1	5
Ag	2	159	0.1	10
WO_3-Ag-WO_3-Ag	–	–	–	200-1-30-10

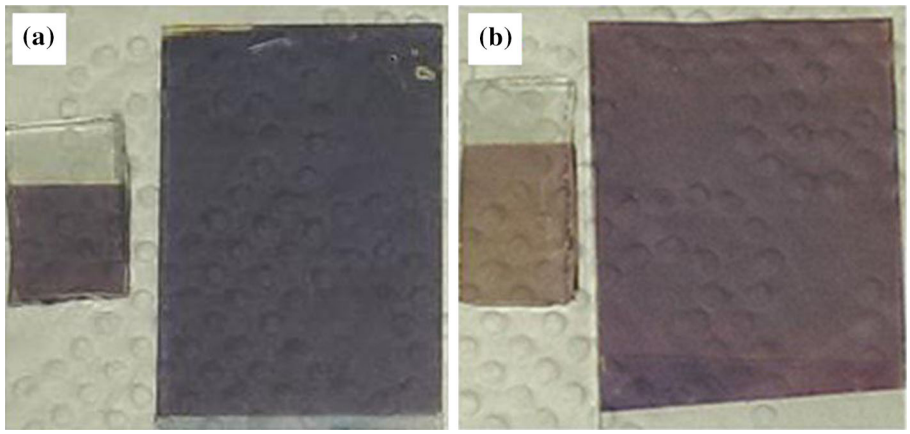

Fig. 1. Multi-layer arrangement of WO_3-Ag-WO_3-Ag at a thickness of 200-1-3-1 nm on FTO and glass: (a) before annealing and (b) post-annealing.

Figure 1a shows the violet-colored EC thin film revealing the multi-layer arrangement of the WO_3-Ag-WO_3-Ag at thicknesses of 200-1-3-1 nm onto FTO and glass. For the crevasse nanoparticles, the post-annealing process was carried out in an electric vacuum oven at 100°C, 200°C and 500°C for 1 min to produce lavender-colored EC thin film (Fig. 1b).

RESULTS AND DISCUSSION

Morphology Studies

The morphology of the post-annealed WO_3-Ag-WO_3-Ag thin film was determined by SEM (Mira; Tescan) and AFM (AP 0100). Figure 2 shows the SEM images of the samples. The sample consisted of canals with hill-like species on the surface (Fig. 2a). For the thin film post-annealed at 100°C, 200°C and 500°C, nanoparticles of Ag (marked) had average grain sizes of 36.5 nm, 35 nm and 33 nm, respectively, in the canals (Fig. 2b, c, and d). This confirms that the structure of the surface was modified by the annealing. Figure 2d shows the presence of luminaries resulting from the high annealing temperature of 500°C.

To better assess morphology, Fig. 3 shows cross-sectional SEM and X-MAP images. Figure 3a shows that the surface has acceptable roughness with adequate porosity in the canaliculated coating to allow the ions to pass. Figure 3b shows the X-MAP of tungsten (green spots), oxygen (blue spots) and silver (red spots) nanoparticles on the surface of the thin film. The sprawl distribution of the present particles can be seen in the WO_3-Ag-WO_3-Ag thin film. Figure 4 shows an EDX of the thin film that confirms the presence of the fundamental elements in a sample and lists the weight and atomic percentages of the components in the structures. As seen, the essential elements of tungsten oxide and silver are present in the EDX spectrum.

Figure 5 shows the topography of the AFM images (FTO-WO_3-Ag-WO_3-Ag) of the composite layers of the sample surface. The surface roughness depended on the deposition substrate and affected the properties of the coatings. As seen, the surface morphology of the tungsten trioxide coating was the smoothest of the composite layers. The symmetrical morphology of the surface at about 7.5 nm had an approximate roughness of 17.8 nm in the hill-like structures seen in the SEM images. The two-dimensional representation and peaks of the three-dimensional representation show that the silver nanoparticles were not uniformly placed on the surface of the tungsten oxide layer at lower deposition times. There was no agglomeration of silver nanoparticles or irregular roughness on the surface.[2–4]

CV Studies

Figure 2 shows the CV spectra of samples in 0.5 M $LiClO_4$-PC solution in the region from − 1.0 V to + 1.0 V versus Ag/AgCl at a scan rate of 100 mV/s. It shows the effect of post-annealing temperature on the FTO-WO_3-Ag-WO_3-Ag composite coatings. All samples exhibit broad peaks of oxidation and decreases in the broad peak caused by intercalation of Li^+ into and deintercalation of Li^+ out from the nanocomposite thin film. The oxidation peak shifted from + 0.1 V to + 0.3 V as the post-annealing temperature increased 100–500°C (Fig. 2). The maximum decay rate for all three temperatures was − 0.15 mA/cm^2. The maximum oxidation current density was 6 mA/cm^2 at a potential of + 0.3 V for an annealing temperature of 200°C, which is two to three times faster than the current flow rate of the thin film at annealing temperatures of 100°C and 500°C.

The area of the cyclic voltammetric curve, the height and position of the broad oxidation peak and the decrease in the broad peak depend on the EC processes in the thin film. Figure 6 shows that increasing the annealing temperature from 100°C to 200°C increased EC activity, the area under the voltammetric cycle curve and the amount of

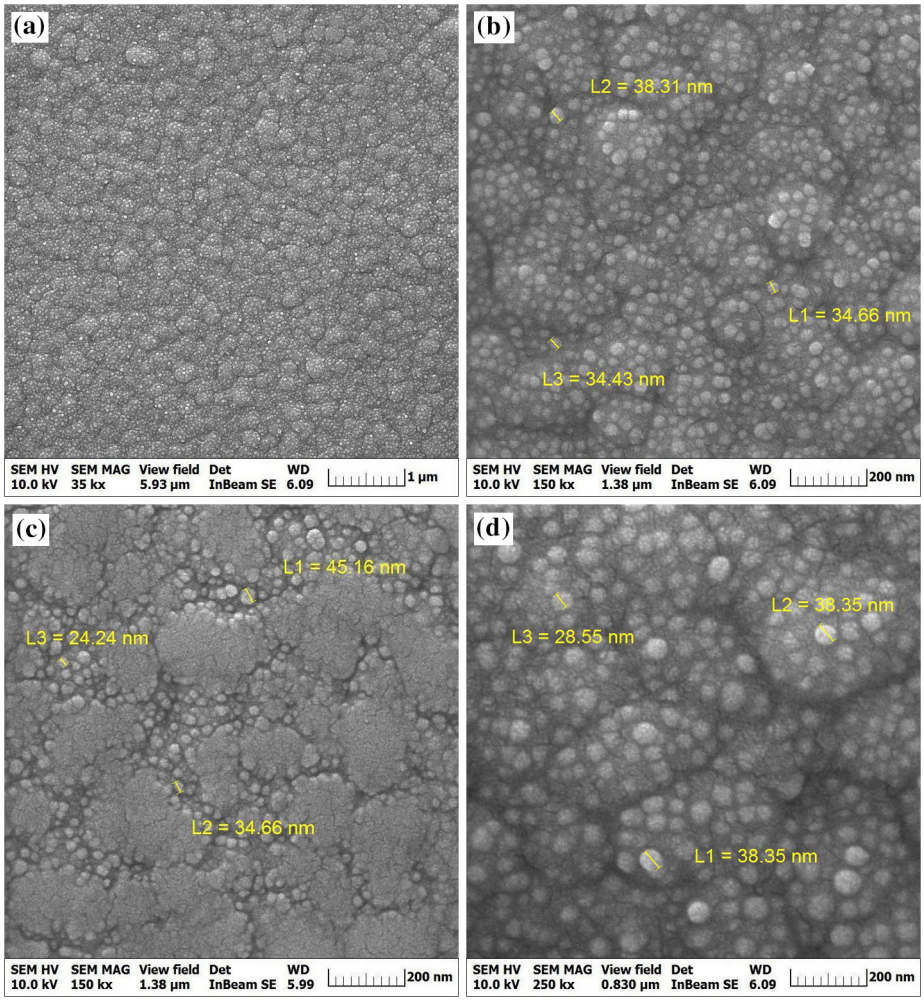

Fig. 2. SEM images of FTO-WO_3-Ag-WO_3-Ag thin film: (a) surface, (b) post-annealed at 100°C, (c) post-annealed at 200°C, and (d) post-annealed at 500°C.

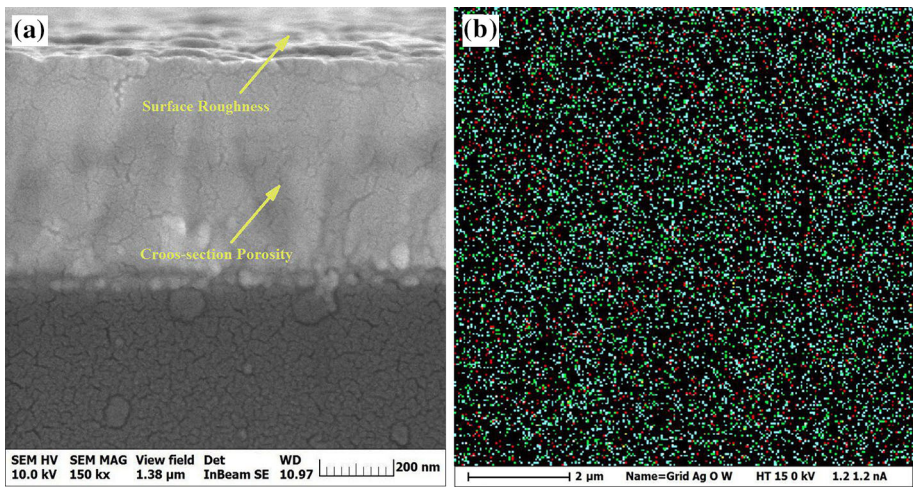

Fig. 3. (a) SEM cross-section. (b) X-Map of EC FTO-WO_3-Ag-WO_3-Ag thin film.

coloration of the sample. With an increase in the annealing temperature from 200°C to 500°C, these values decreased because adhesion of the crystals increased, decreasing the electrolyte penetration in the layer, as shown in the SEM image. The sample at a post-annealing temperature of 200°C shows

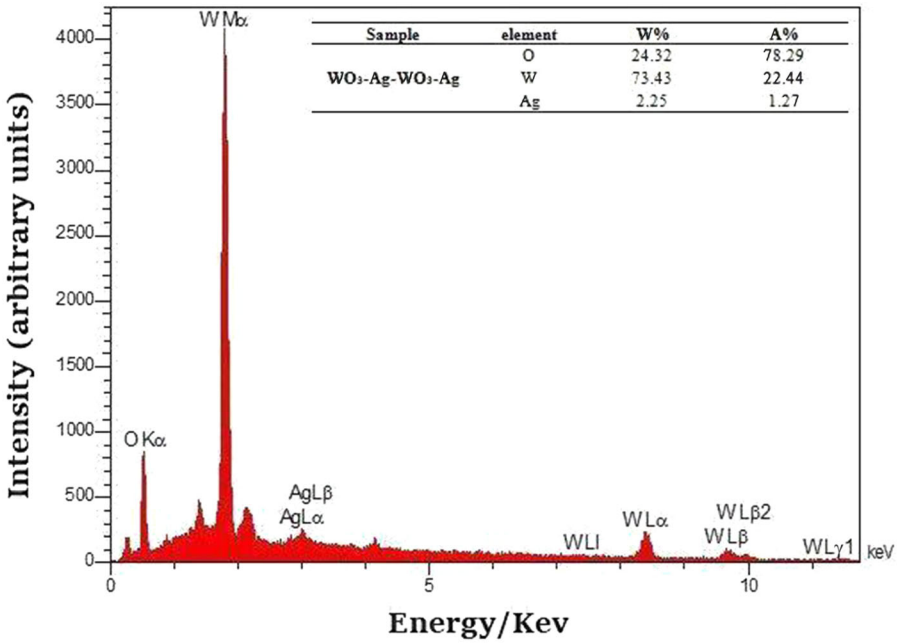

Fig. 4. EDX spectrum of images of FTO-WO_3-Ag-WO_3-Ag EC thin film.

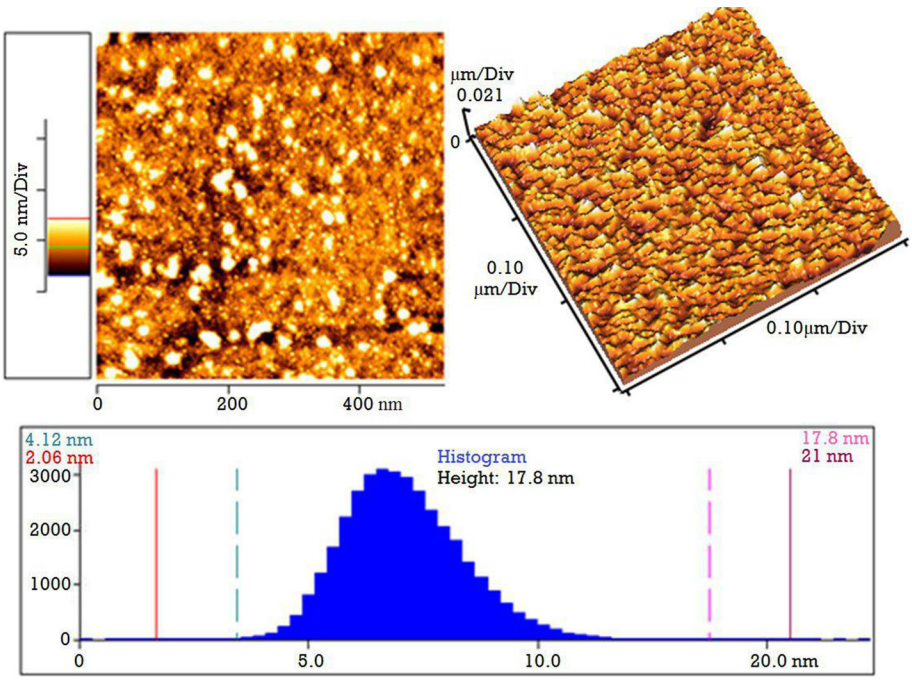

Fig. 5. AFM image of FTO-WO_3-Ag-WO_3-Ag EC thin film.

conductivity for the positive and negative potentials. The conductivity of the sample with an annealing temperature of 500°C reduced sharply, which is not acceptable for an ECD.[3]

Optical Properties

The optical qualities of the film were investigated using a UV–Vis spectrophotometer (Shimadzu 210). Figure 7 shows the variation in optical transmittance $T(\lambda)$ of the WO_3-Ag-WO_3-Ag coatings deposited over the glass substrate at different post-annealing temperatures versus the wavelength (300–800 nm) at DC voltages of − 1.0 to + 1.0 V. The maximum optical transmittance of the bleached sample annealed at 100°C was 77.63%, and the minimum optical transmittance of the colored sample was 42.69% at the same wavelength. The sample

that was annealed at 200°C showed excellent results; optical transmittance in the bleached state was 82.53% and minimum optical transmittance in the colored state was 38.74% at the same wavelength. The maximum and minimum outcomes for a sample annealed at 500°C were 69.27% and 51.43%, respectively. Table II shows the differences in transmittance (ΔT%) of samples to be 34.94, 43.79 and 17.84 at post-annealing temperatures of 100°C, 200°C and 500°C, respectively, at the same and optimal wavelength (632.8 nm). The following relationship expresses the optical band gap:

$$\alpha h\upsilon = A\left(h\upsilon - E_g\right)^n \quad (1)$$

where $h\upsilon$ is the photon energy, E_g is the optical energy band gap of the material and n is the power which describes transitions in which n = 1/2 and 3/2 for direct allowed and forbidden transitions, respectively.[30–33]

The direct band gap of the thin film was delimited by extrapolating the linear part of $(\alpha h\upsilon)^2$ upon the photon energy plan as shown in Fig. 8. The calculated values of E_g (3.62 eV, 3.43 eV and 2.86 eV) show that the increase of post-annealing temperatures from 100°C to 200°C increased the optical band gap. It can be concluded that an increase in post-annealing temperatures from 200°C to 500°C will decrease the crystallization of the thin film after high-temperature post-annealing. Other researchers have reported similar trends.[4,34]

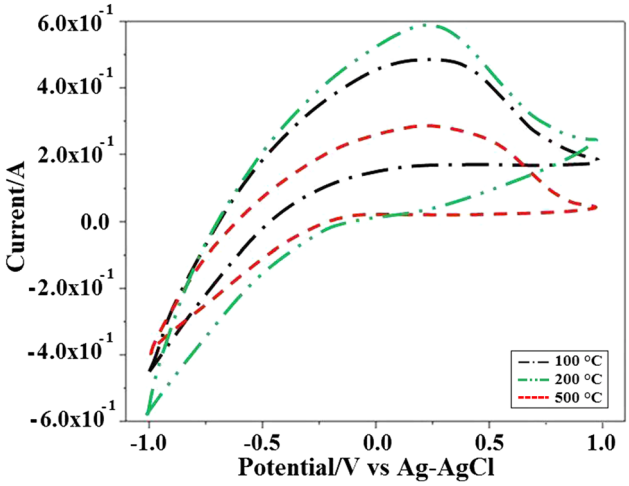

Fig. 6. Cyclic voltammogram of EC thin film at post-annealing temperatures of 100°C, 200°C, and 500°C.

EC Properties

The RT and coloration switching response are the controlling parameters of EC properties. RT is computed as the time required for a 90% change

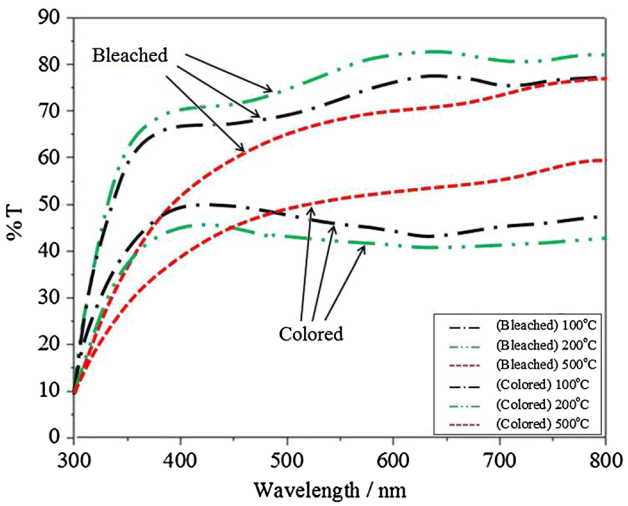

Fig. 7. Visible transmittance spectra of WO_3-Ag-WO_3-Ag EC thin film at post-annealing temperatures of 100°C, 200°C, and 500°C.

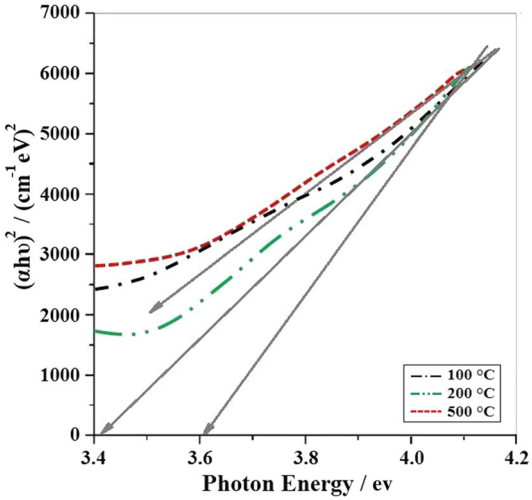

Fig. 8. Plot of $(\alpha h\upsilon)^2$ versus photon energy $h\upsilon$ of WO_3-Ag-WO_3-Ag EC thin film at post-annealing temperatures of 100°C, 200°C, and 500°C.

Table II. Optical and electrochromic properties of FTO-WO_3-Ag-WO_3-Ag thin films different post-annealing temperatures

Sample	DC voltage steps (V)	T_b (%)	T_c (%)	ΔT (%)	E_g (ev)	CE ($cm^2\ C^{-1}$)	τ_B (s)	τ_c (s)
100°C	+ 1.0 ↔ − 1.0	77.63	42.69	34.94	3.62	65.4	11.2	9
200°C	+ 1.0 ↔ − 1.0	82.53	38.74	43.79	3.43	75.2	8.2	7.4
500°C	+ 1.0 ↔ − 1.0	69.27	51.43	17.84	2.86	34.1	21.8	12.5

in the full transmittance modulation at a proper wavelength with the highest difference in transmittance (632.8 nm). Figure 9 shows the current transient response and corresponding switching curves at 632.8 nm for the WO_3-Ag-WO_3-Ag coatings deposited over an FTO substrate at different post-annealing temperatures in 0.5 M $LiClO_4$-PC electrolyte. DC voltage steps from − 0.1 V to + 1.0 V were used for all samples. Subsequently, the RT for the samples (100°C, 200°C and 500°C) to move from a bleached to a colored state were estimated to be 11.2 s, 8.2 s and 21.8 s, and from colored to bleached states to be 9 s, 7.4 s and 12.5 s. The current density of the EC film at continuous switching from + 1.0 V to − 1.0 V and − 1.0 V to + 1.0 V is shown in Figs. 6, 7 and 9. Comparison of the interchanged charge (area under the curve) in a post-annealed sample at 200°C was greater than for the other samples. This effect was accompanied by the greatest difference in transmittance for this sample, indicating it is a better sample for this structure.[2–4]

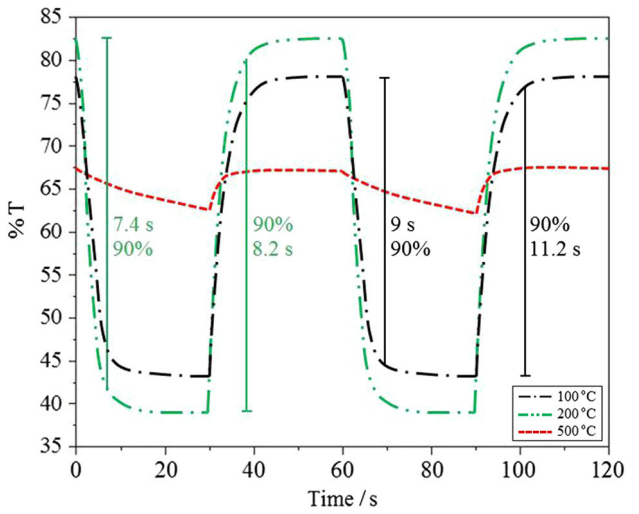

Fig. 9. RT of WO_3-Ag-WO_3-Ag EC thin film post-annealing at 100°C, 200°C, and 500°C.

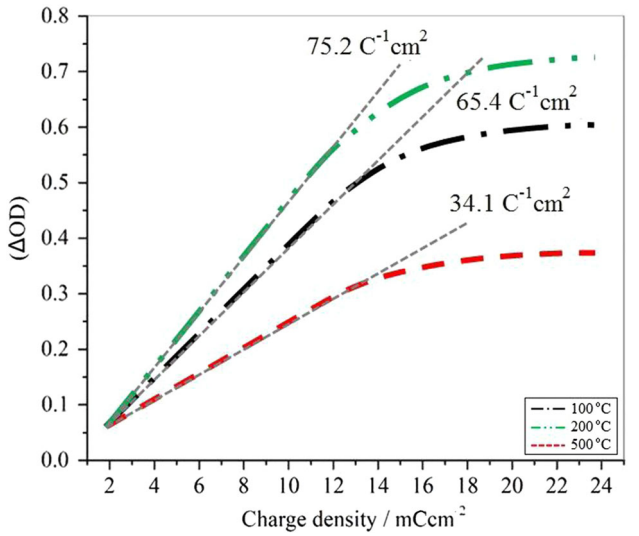

Fig. 10. CE of WO_3-Ag-WO_3-Ag EC thin film post-annealing at 100°C, 200°C, and 500°C.

CE is another critical property of EC materials. It is obtained from the slope of the variation in optical density (ΔOD) between two agreeable optical states at a specific wavelength (632.8 nm) versus the similar charge density (Q) per unit area (A). This definition is expressed in Eqs. 2 and 3, where T_c and T_b are the colored and bleached transmittances of the EC film, respectively.[3,4]

$$CE = \Delta OD/(Q/A) \quad (2)$$

$$\Delta OD(\lambda) = \log\frac{T_b}{T_c} \quad (3)$$

The CE of samples were calculated to be 75.2 $cm^2\ C^{-1}$, 65.4 $cm^2\ C^{-1}$ and 34.1 $cm^2\ C^{-1}$ for FTO-WO_3-Ag-WO_3-Ag thin film at post-annealing temperatures of 100°C, 200°C and 500°C (Fig. 10). The optical and EC properties of the samples were investigated. Table II shows that the optical (ΔT%) and EC performance (CE and RT) increased in the sample at 200°C compared with the other post-annealing temperatures (100°C and 500°C). This could result from the absence of oxidation of silver and high-level nanocomposites that formed and, in turn, caused the number of atoms at the surface to be higher than the number of atoms in the bulk of the sample.[3]

CONCLUSIONS

The WO_3 and Ag nanoparticles were successfully deposited on glass and FTO-coated glass substrate using the PVD method. The FTO-WO_3-Ag-WO_3-Ag thin film was post-annealed at 100°C, 200°C and 500°C in a vacuum. It could be concluded that three

Table III. Electrochromic properties comparison of (WO_3), (WO_3-Ag), and (WO_3-Ag-Wo_3-Ag post-annealed at 200°C) thin films

Sample	DC voltage steps (V)	ΔT (%)	CE ($cm^2\ C^{-1}$)	τ_c (s)	τ_B (s)	Color	Ref.
WO_3	+ 1.0 ↔ − 1.0	35.46	63.5	5.3	6.9		3
WO_3-Ag	+ 1.0 ↔ − 1.0	39.65	74.2	4.4	5.3		3
WO_3-Ag-Wo_3-Ag	+ 1.0 ↔ − 1.0	43.79	75.2	7.4	8.2		–

steps are required to improve the ECD. First is the use of tungsten oxide nanoparticles as an *n*-type semiconductor for the cathode EC material in the ECD. Second is the use of nano-sized silver as the metal in the electron trap centers to facilitate charge departure in ECD. Third is the optimal post-annealing temperature required to cause the silver nanoparticles to penetrate the tungsten oxide on the surface of the thin film. The optical and EC properties of the samples were compared with similar types of film (WO_3 and WO_3-Ag).

Table III shows the increase in the optical and EC performance in a WO_3-Ag-WO_3-Ag nanocomposite post-annealed at 200°C compared to the WO_3 and WO_3-Ag nanocomposites. Notably, the change in transmittance (ΔT) and CE of this sample increased to 43.79% and 75.2 $cm^2\ C^{-1}$, respectively. Moreover, the response times for bleached to colored (7.4 s) and vice versa (8.2 s) for the sample post-annealed at 200°C indicate a good candidate for use in ECDs. These values are suitable for EC smart windows.

REFERENCES

1. P. Yang, P. Sun, and W. Mai, *Mater. Today* 19, 394 (2016).
2. S. Hoseinzadeh, A. Bahari, R. Ghasemiasl, and A.H. Ramezani, *J. Mater. Sci. Mater. Electron.* 28, 14855 (2017).
3. S. Hoseinzadeh, A. Bahari, R. Ghasemiasl, and A.H. Ramezani, *J. Mater. Sci. Mater. Electron.* 28, 14446 (2017).
4. H. Najafi-Ashtiani, A. Bahari, S. Gholipour, and S. Hoseinzadeh, *Appl. Phys. A* 124, 24 (2018).
5. C.G. Granqvist, S. Green, G.A. Niklasson, N.R. Mlyuka, S. von Kræmer, and P. Georén, *Thin Solid Films* 518, 3046 (2010).
6. V.R. Buch, A.K. Chawla, and S.K. Rawal, *Mater. Today Proc.* 3, 1429 (2016).
7. N. Tripathi, L.D. Bell, S. Nikzad, M. Tungare, P.H. Suvarna, and F.S. Sandvik, *J. Electron. Mater.* 40, 382 (2011).
8. A. Bahari and M. Shahbazi, *J. Electron. Mater.* 45, 1201 (2016).
9. H. Najafi-Ashtiani, A. Bahari, and S. Ghasemi, *Organ. Electron.* 37, 213 (2016).
10. P. Kumar, K.S. Narayan, S. Guha, and F. Shahedipour-Sandvik, *Organ. Electron.* 14, 2818 (2013).
11. R. Gholipur, Z. Khorshidi, and A. Bahari, *ACS Appl. Mater. Interfaces* 9, 12528 (2017).
12. F. Shahedipour-Sandvik and B.W. Wessels, *Appl. Phys. Lett.* 76, 3011 (2000).
13. X.A. Cao, K. Topol, F. Shahedipour-Sandvik, J. Teetsov, P.M. Sandvik, S.E. LeBoeuf, A. Ebong, J.W. Kretchmer, E.B. Stokes, S. Arthur, and A.E. Kaloyeros, in *Proceedings of SPIE 4776, Solid State Lighting II* (2002).
14. C.P. Cheng, Y. Kuo, C.P. Chou, C.H. Cheng, and T.P. Teng, *Appl. Phys. A Mater. Sci. Process.* 116, 1553 (2014).
15. K.J. Patel, C.J. Panchal, M.S. Desai, and P.K. Mehta, *Mater. Chem. Phys.* 124, 884 (2010).
16. R. Baetens, B.P. Jelle, and A. Gustavsen, *Sol. Energy Mater. Sol. Cells* 94, 87 (2010).
17. Y. Guo, X. Quan, N. Lu, H. Zhao, and S. Chen, *Environ. Sci. Technol.* 41, 4422 (2007).
18. I.C. Amaechi, A.C. Nwanya, P.U. Asogwa, R.U. Osuji, M. Maaza, and F.I. Ezema, *J. Electron. Mater.* 44, 1110 (2015).
19. A.H. Ramezani, S. Hoseinzadeh, and A. Bahari, *J. Inorg. Organomet. Polym*. First Online: 02 January (2018).
20. C.G. Granqvist, *Sol. Energy Mater. Sol. Cells* 99, 1 (2012).
21. V.V. Ganbavle, J.H. Kim, and K.Y. Rajpure, *J. Electron. Mater.* 44, 874 (2015).
22. S.-H. Park, S.-M. Lee, E.-H. Ko, T.-H. Kim, Y.-C. Nah, S.-J. Lee, J.H. Lee, and H.-K. Kim, *Sci. Rep.* 6, 33868 (2016).
23. R.R. Kharade, S.S. Mali, S.P. Patil, K.R. Patil, M.G. Gang, P.S. Patil, J.H. Kim, and P.N. Bhosale, *Electrochim. Acta* 102, 358 (2013).
24. H. Li, Y. Lv, X. Zhang, X. Wang, and X. Liu, *Sol. Energy Mater. Sol. Cells* 136, 86 (2015).
25. K.W. Park, *Electrochim. Acta* 50, 4690 (2005).
26. H. Huang, J. Tian, W.K. Zhang, Y.P. Gan, X.Y. Tao, X.H. Xia, and J.P. Tu, *Electrochim. Acta* 56, 4281 (2011).
27. C. Feng, S. Wang, and B. Geng, *Nanoscale* 3, 3699 (2011).
28. D. Dastan, S.L. Panahi, and N.B. Chaure, *J. Mater. Sci. Mater. Electron.* 27, 12291 (2016).
29. D. Dastan and A. Banpurkar, *J. Mater. Sci. Mater. Electron.* 28, 3851 (2016).
30. S.B. Upadhyay, R.K. Mishra, and P.P. Sahay, *Ceram. Int.* 42, 15601 (2016).
31. M. Reghima, A. Akkari, C. Guasch, and N. Kamoun-Turki, *J. Electron. Mater.* 44, 4392 (2015).
32. S. Karthika, V. Prathibha, M.K.A. Ann, V. Viji, P.R. Biju, and N.V. Unnikrishnan, *J. Electron. Mater.* 43, 447 (2014).
33. V. Vidyadharan, P. Vasudevan, S. Karthika, C. Joseph, N.V. Unnikrishnan, and P.R. Biju, *J. Electron. Mater.* 44, 2754 (2015).
34. H. Wei, J. Zhu, S. Wu, S. Wei, and Z. Guo, *Polymer (United Kingdom)* 54, 1820 (2013).